Investigation of the impact of long-range aerosol transport on air quality: using MERRA2 aerosol reanalysis and multi-platform observations

Sheng-Po Chen[1,2], Wei-Ting Hung[2], Cheng-Hsuan (Sarah) Lu[2]

[1]Center for Environmental Studies, National Central University
[2]Atmospheric Sciences Research Center, University at Albany, State University of New York

Abstract

While the surface air quality has been improved by regulating effective regulatory policies and emission reduction strategies to control anthropogenic emissions, biogenic emissions, in contrast, cannot be manually eliminate and tended to affect the environment in decades. In this study, multiple datasets including satellite and ground-based observations, trajectory modeling and the Modern-Era Retrospective analysis for Research and Applications Version 2 (MERRA2) aerosol reanalysis were utilized to investigate the impact of long-range aerosol transport on air quality. One case characterized the long-range transport of smoke plumes and their air quality impact on New York State, U.S.A., and the other case showed the long-range transport of Asian dust together with Chinese haze and their air quality impact on Northern Taiwan. Both cases demonstrate that meteorological pattern plays a critical role in determining whether the long-range aerosols staying aloft along the transport path or being mixed (or retrained) down to the ground, further affecting surface air quality. The aerosol subsidence could potentially affect the effectiveness of emission controls and pollutant reductions.

Key word: MERRA2, aerosol reanalysis, long-range aerosol transport, remote sensing

1. Introduction

Dust is one of the long-range transport aerosols reported to transport eastward across long distance to Taiwan. Gobi Desert and Taklamakan Desert are two major dust source regions in East Asia *[Tsai et al., 2008; X Wang et al., 2004]*. Strong surface winds induced by frontal systems lift coarse particles (PM_{10}) from dry surface to upper layer *[Hsu et al., 2012; C-M Liu et al., 2006; M Liu et al., 2003; Tsai et al., 2014]*. Taklamakan desert is located at the center of the Tarim Basin with elevated mountain ranges (>5000 m) surrounded. Dust outbreaks from Taklamakan desert only affect neighboring areas *[X Wang et al., 2004]*. However, when Taklamakan dust is entrained to high altitudes, it can escape the basin and transport across the Pacific to reach the United States *[Chen et al., 2018]* and even deposit on Greenland ice cap *[Bory et al., 2003]* . In contrast, over Gobi Desert, mineral aerosols are found to travel eastward to Korea, Japan and even across the Pacific, or southeastward to South Asia, Hong Kong and Taiwan, under different synoptic circulations *[Jung et al., 2017; Mori et al., 2003; Tsai et al., 2008]*. Since Asian dust is mainly generated during spring (March to May), long-range transported Asian dust events have less frequency and make smaller effect in Taiwan during wintertime, compared to Chinese haze *[Lin et al., 2012; S-H Wang et al., 2016]*.

In contrast to dust, Biomass burning is one significant source for trace gases and aerosols *[Crutzen and Andreae, 1990; Crutzen et al., 1979; Levine et al., 1995; Seiler and Crutzen, 1980]*. Globally, open biomass burning contributes 74% and 42% of organic carbon (OC) and black carbon (BC) emissions, respectively *[Bond et al., 2004]*. Smoke aerosols, once emitted, can be injected into the free troposphere [*Leung et al.*, 2007]. Aerosol aloft can be transported for a long distance and affect air quality at local, regional, and even intercontinental scales [*Bertschi and Jaffe*, 2005; *P R Colarco et al.*, 2004; *Damoah et al.*, 2004; *Forster et al.*, 2001; *Jaffe et al.*, 2004; *Petzold et al.*, 2007; *Wu et al.*, 2018].

For the past decades, there have been multiple datasets which can be used to analyze the long-range transport of dust and smoke. Understanding and quantifying the influence of transported dust and smoke plumes on air quality is critical for cost effective planning. In this study, we examine two dust/smoke transport events in Northern Taiwan and New York State (NYS), U.S. The NASA Modern-Era Retrospective analysis for Research and Applications, Version 2 (MERRA-2) aerosol reanalysis, back-trajectory analysis, and multi-platform observations were utilized to characterize Asian dust and wildfire smoke transports and their impacts on local air quality in Northern Taiwan and NYS, U.S.

2. Methodology and dataset

2.1 Trajectory analysis

The Hybrid Single-Particle Lagrangian Integrated Trajectory (HYSPLIT) Model was developed by NOAA Air Resources Laboratory (ARL). It is one of the most

extensively used atmospheric dispersion models for the study of air parcel trajectories *[Draxler and Rolph, 2012; Randles et al., 2017; Stein et al., 2015]*. In this study, HYSPLIT Version 4 is used to compute the backward trajectories of air parcels, identify the possible source regions of smoke aerosols, and establish source-receptor relationships. Three-dimensional meteorological inputs are taken from the NCEP North American Mesoscale Model (NAM) (CDAS) by NCEP. The NAM sigma-pressure hybrid (NAMS) data over CONUS contain hourly meteorological fields with a spatial resolution 12 km horizontally.

2.2 Aerosol reanalysis

The Modern-Era Retrospective analysis for Research and Applications Version 2 (MERRA-2) is a satellite era (1980 onward) reanalysis system from NASA Global Modeling Assimilation Office (GMAO) *[Gelaro et al., 2017]*. As a step toward a fully integrated Earth systems analysis, meteorological and aerosols observations are jointly assimilated. The aerosol module in MERRA-2 is an online version of the Goddard Chemistry, Aerosol, Radiation, and Transport model (GOCART) *[P Colarco et al., 2010]*. Five aerosol species are simulated, including mineral dust (DU) with 5 size bins, sea salt (SS) with 5 size bins, sulfate (SU), BC and OC. The MERRA-2 aerosol reanalysis assimilates aerosol observations from Advanced Very High Resolution Radiometer (AVHRR), the Moderate Resolution Imaging Spectroradiometer (MODIS), Multi-angle Imaging SpectroRadiometer (MISR), and NASA AErosol RObotic NETwork (AERONET). Emissions of biomass burning are obtained from Quick Fire Emissions Data Version 2 based on MODIS Fire Radiative Power (QFED2) *[Darmenov and da Silva, 2015]*. Descriptions and assessment of MERRA-2 aerosol reanalysis can be found in Randles et al. *[Randles et al., 2017]* and Buchard et al. *[Buchard et al., 2017]*.

The output collection of MERRA-2 reanalysis is on the regular 0.625° x 0.5° longitude-by-latitude grid and 72 levels from the surface to 0.01 hPa. The MERRA-2 data can be downloaded from the NASA GIOVANNI web server (https://giovanni.gsfc.nasa.gov/giovanni/).

2.3 Satellite products

The Visible Infrared Imaging Radiometer Suite (VIIRS), a scanning radiometer, measures cloud and aerosol properties in the atmosphere and provides observations of land, cryosphere, and ocean surface. It is onboard the Suomi National Polar-orbiting Partnership (Suomi-NPP, launched in 2011) and NOAA-20 (formerly Joint Polar Satellite System (JPSS)-1, launched in 2017). The advanced VIIRS Enterprise Processing System (EPS), implemented in July 2017, is an advanced retrieval algorithm to replace the Environmental Data Record (EDR). The overall accuracy (retrieval bias) for high quality AOD over land is 0.018 and 0.030 over water, and the overall precision (standard deviation of retrieval errors) for high quality AOD over land is 0.112 and 0.046 over water. Details of the VIIRS EPS AOD algorithms are described in Laszlo and Liu *[Laszlo and Liu, 2016]* and Zhang et al. *[Zhang et al., 2016]*. The EPS data analyzed in this study is pre-operational product provided by NOAA National Environmental Satellite, Data, and Information Service (NESDIS) for scientific collaborations. In this study, the daily VIIRS EPS Aerosol Optical Depth (AOD) at 550 nm, daily gridded at 1°x1°, is used for the characterization of smoke cases as well as inter-comparison of aerosol spatial distributions with MERRA-2.

2.4 Ground-based observations

For the case study in Northern Taiwan, the Wanli site (25.18° N, 121.69° E; 27 m a.s.l.) is one of the four background sites as part of the Taiwan Air Quality Monitoring Network (http://taqm.epa.gov.tw) operated by the Taiwan Environmental Protection Administration [*EPA*]. It is around 200 m to the shore, thus is considered the first detection of Asian continental outflow. Note that Wanli site is about 100 m away from a main road and could under the influence of local pollutants during rush hours. Metone BAM 1020 continuous particulate monitor is used for PM measurement. Metone 014A wind speed sensor and 024A wind direction sensor are used for wind measurements. Instruments are deployed at 3–15 m above the ground and undergo daily automatic zero and span checks. In-situ air quality measurements, consisting of hourly total PM_{10} and total $PM_{2.5}$ mass concentration, and wind observations taken at Wanli site were used in this study.

For the case study in U.S., the surface $PM_{2.5}$ and gaseous pollutants observations at air quality stations (AQS) in NYS are operated and maintained by NYS Department of Environmental Conservation (DEC). In this study, the surface hourly $PM_{2.5}$ mass concentration by the Federal Equivalent Method (FEM) instruments are used. The surface meteorological fields, including wind fields and precipitation amounts, in NYS are provided by NOAA National Centers for Environmental Information (NCEI) Integrated Surface Database (ISD). Global hourly and synoptic measurements from numerous sources are collected by ISD from more than 35,000 stations worldwide, including wind fields, temperature, dew point, cloud data, sea level pressure, altimeter setting, station pressure, visibility, precipitation amounts, snow depth, etc. Details of ISD quality control can be referred to Smith et al. *[Smith et al., 2011]*.

3. Case studies

3.1 Dust-dominated transport event over Northern Taiwan

A transported high $PM_{2.5}$ event, from Feb. 28 2300 UTC to 29 1000 UTC in 2016, was observed with peak $PM_{2.5}$ concentration of 60 μg m^{-3} at 29 0700 UTC. Dust showed higher surface mass concentration (**Fig. 1a**) than sulfate and the ratio of DU/(DU+SU) was 0.68. Therefore, this event was defined as a dust-dominated transported event. According to backward trajectories (**Fig. 1b**) and surface weather maps (not shown), two air

mass contributed to the event simultaneously. One transported from the north, shown as the trajectory released at 375 m (blue path in **Fig. 1b**), is associated with surface high pressure system. Another air mass, shown as the trajectory released at upper level as 1000 m (red path in **Fig. 1b**), is traced back to the west and attributed to an eastward frontal system. **Fig. 1c** and **1d** are timeseries of MERRA-2 sulfate/dust vertical profiles following the backward trajectories at different release levels. The trajectory at 375 m passed through relative clean regions and the vertical profiles (**Fig. 1c**) did not show significant dust signals except for the last day when dust plume settled down to the surface. In contrast, vertical aerosol profiles along with the trajectory released at 1000 m (**Fig. 1d**) exhibited that dust lifted to upper level of 700–800 hPa over the source region, transported eastward, then descended to the surface and mixed with sulfate in the last day before reaching Northern Taiwan.

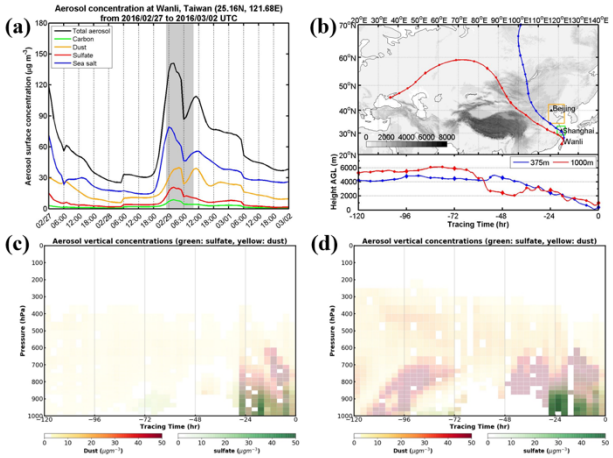

Fig. 1. (a) Timeseries of MERRA-2 surface aerosol mass concentrations at Wanli from Feb. 27 to Mar. 2, 2016. Gray shading represents event period according to in-situ $PM_{2.5}$ observation. (b) Five-day backward trajectories ending at Wanli at 0700 UTC on Feb. 29, 2016 when peak surface $PM_{2.5}$ concentration occurred. Blue and red lines are trajectories released at 375 m and 1000 m, respectively. Timeseries of MERRA-2 aerosol vertical profiles following the backward trajectories released at (c) 375 m and (d) 1000 m. Red and green shadings show dust and sulfate mass concentrations, respectively.

Fig. 2 are geopotential heights at 700 hPa with (a) total column aerosol optical depth (AOD) and (b) aerosol surface mass concentrations based on MERRA-2 reanalysis. High dust loading occurred over Gobi Desert (northwestern China). Dust aerosols moved eastward driven by the trough at 700 hPa and mixed with sulfate aerosols near the coast. From **Fig. 2a**, there is a significant dust plume, shown as red colors with high dust concentrations, transports cross continental Asia. As for surface concentrations (**Fig. 2b**), although there was no significant west-to-east transported dust outflow, relative high values were found over east coast regions. Deep troughs at 700 hPa provided efficient downwind motion, bringing aloft dust to the surface and pushed mixed aerosols southeastward to Northern Taiwan subsequently.

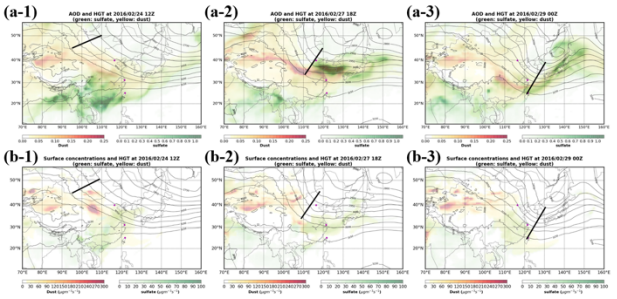

Fig. 2. Geopotential height at 700 hPa (contour) with (a) total AOD and (b) surface aerosol mass concentrations from Feb. 24-29, 2016. Red and green shadings show dust and sulfate mass concentrations, respectively. Bold black lines show where low-level troughs located.

3.2 LRT smoke events in New York State

To investigate the impact of long-range smoke transport on air quality in New York State (NYS), the smoke event that occurred on Sep. 5 were analyzed. In **Fig. 3a**, the elevated AOD (> 0.8) were observed by VIIRS spread over Northwest U.S., Rocky Mountain States, the Gulf States, Mid-Atlantic, and Northeast. The OMPS AI (**Fig. 3b**) greater than 4 was detected over NYS on Sep. 5, suggesting the presence of absorbing aerosols in this region. The CATS data in **Fig. 3c** show that the aloft smoke plumes were located at 3-6 km. The smoke plume over NYS was also shown by AIRS integrated CO column mass (**Fig. 3d**), as elevated CO column mass spanned from the western U.S. to NYS. VIIRS, OMPS and AIRS all presented a consistent and qualitative picture of aerosol distribution across the CONUS. It is reasonable to assume high OMPS AI values were mainly due to smoke aerosols because there is no significant source of dust or volcanic ash for CONUS during the study period.

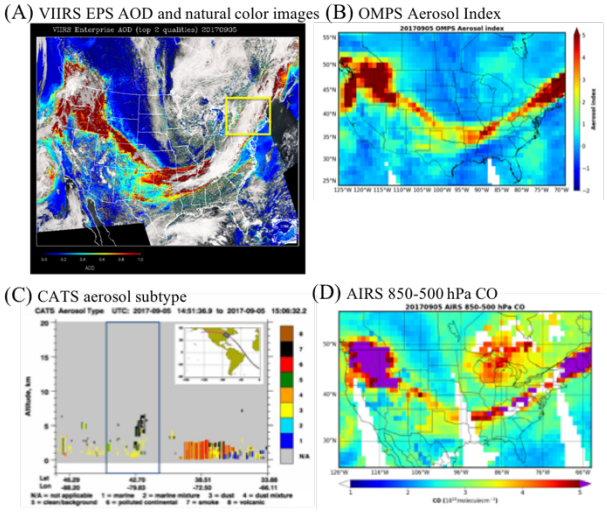

Fig. 3. Satellite retrievals for Sep. 5 smoke.

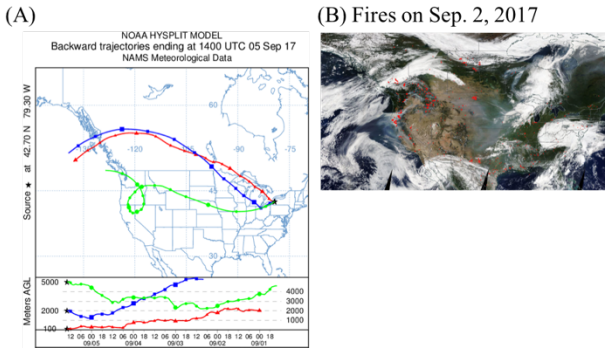

Fig. 4. Source identification of two smoke events by 5-day HYSPLIT backward trajectories.

Fig. 4a presented the HYSPLIT 5-day backward trajectories and time-height profiles for the two smoke cases. The back trajectories released at 5-km for the 2 cases were both traced back to the Northwest U.S. The Sep. 5 smoke event started from the west U.S.-Canada border and transported across the continent toward eastern U.S. The corresponding VIIRS fire and thermal anomalies were shown in **Fig. 4b**. The date of VIIRS images were chosen according to the HYSPLIT backward trajectories for the sources in the western U.S. The transport patterns by HYSPLIT and the sources by VIIRS thermal anomalies were consistent with the spatial extent of smoke depicted by satellites, i.e., there were common large fires in Northern Rocky Mountains detected for both smoke events.

The MERRA2 Altitude-averaged cross-sections of aerosol mixing ratios (MMR) and omega winds (from 39°N to 50°N) for two smoke events were shown in **Fig. 5**. For the Sep. 5 smoke event, the smoke aerosols were found around Montana (at 105°W~115°W) and Oregon (at 125°W). Once emitted from the fire, the smoke plumes elevated up to 500 hPa by thermal convection. The 500 hPa temperature was 295 k from surface to 500 hPa. The smoke plumes in Alberta, Canada, mixed with smoke plume in Oregon, moved southward to 42°N, and stayed aloft up to 500 hPa. As the smoke plumes kept moved eastward, the smoke plumes at source regions in the west U.S. raised from surface to 500 hPa on Sep. 4 due to high-pressure at 105°W~125°W. On Sep. 5, an elevated smoke plumes approached NYS and kept up with the frontal system. Due to the frontal system along with high baroclinicity above surface, the omega at NYS region (at 80°W~70°W) showed an upward motion (positive values stand for upward motion). This upward forcing kept the aloft smoke plumes suspended at above 700 hPa. However, after Sep. 5 18z, as the cold frontal passed central NYS and moved to the east coast U.S., the strong convective transport with downward motion located at southeast NYS (close to New York City) on Sep. 5. Hence, the elevated smoke plumes mixed down to the surface.

On Sep. 5, there were three sites with $PM_{2.5}$ observations over 35 μg m^{-3}: two urban sites, CCNY (45.2 μg m^{-3}) and NBURG (99.6 μg m^{-3}), in NYC, and one rural site, Pinnacle State Park (43.3 μg m-3), in the south of NYS.

Taking the NBURG site as an example (**Fig. 6a**) the peak $PM_{2.5}$ were shown on Sep. 6, along with precipitations observed at nearby ISD Dutchess County Airport (KPOU) site (**Fig. 6b**). As the cold frontal system moved forward to the east coast U.S., the wind directions turned from southerly to northeasterly.

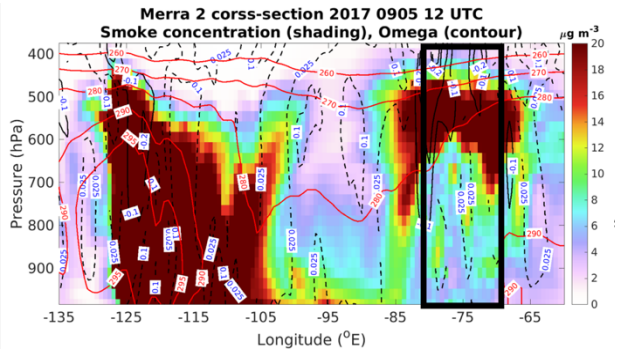

visible over a

Fig. 5. Altitude-averaged cross-sections (39-50°N) of MERRA-2 aerosol mass mixing ratios along with omega winds. Positive contours are downward motions, and vice versa. Black rectangular covers NYS latitudes.

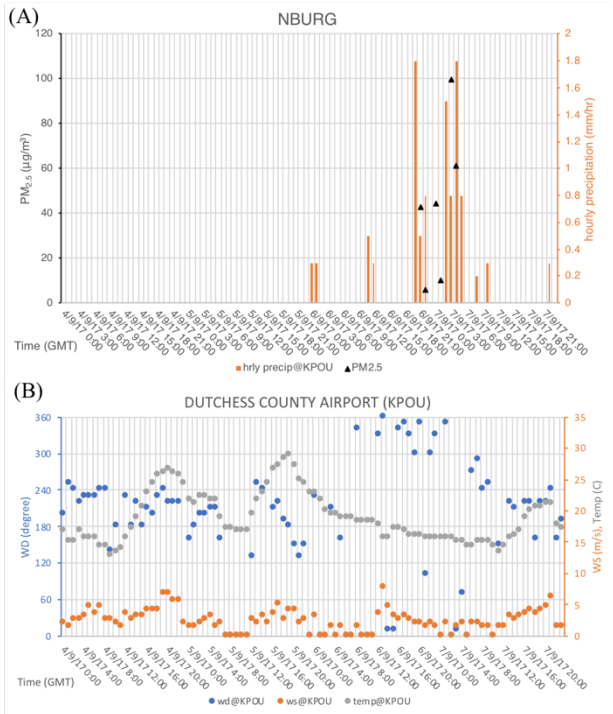

Fig. 6. Timeseries of $PM_{2.5}$ at NBURG site and its neighboring airport site (KPOU).

The MERRA2 aerosol fields together with meteorological fields were also displayed for the NBURG site (**Fig. 7**). On Sep. 5, as the cold-front moved to NYS, the smoke plume resided at 3-4 km did not reach the ground due to updraft near surface (**Fig. 7b**). After Sep. 6, the cold front kept moving. The precipitations at NBURG occurred before Sep. 6 6z (**Fig. 7a**), therefore started to washout smoke plumes (originally the OC MMR were as high as 0.4 x 10^{-7} kg kg^{-1} at Sep. 5 6z, but became 0.05 x 10^{-7} kg kg^{-1} after Sep. 6 12z, **Fig. 7b**). At the NBURG site, the originally aloft

OC at 3-4 km were downward to the surface after Sep. 6 6z, and therefore the high $PM_{2.5}$ speciated from OC after Sep. 6 12z (**Fig. 7a**). The magnitudes of MERRA2 reanalysis aerosols and meteorological fields may not always be consistent with the observed values, but the time line of the cold-front reaching and passing by NYS along with the evolution of smoke plumes aloft was assured.

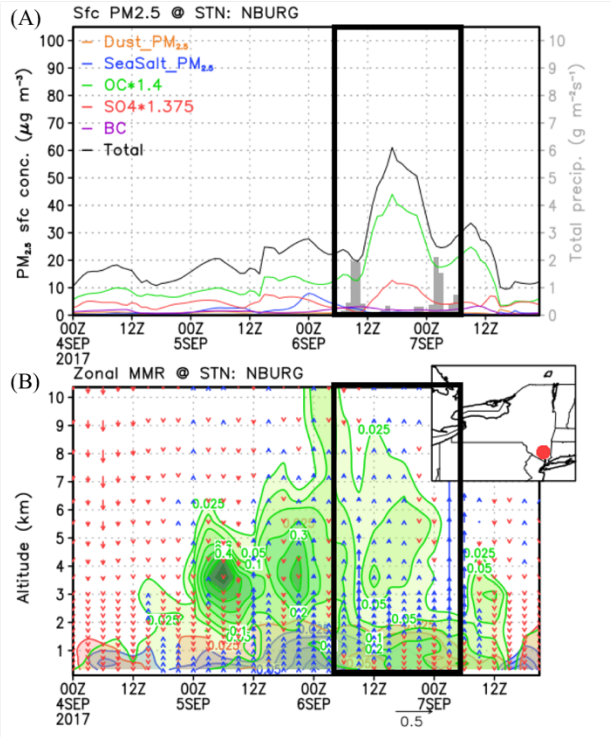

Fig. 7. Surface speciated $PM_{2.5}$ and vertical MMR (10^{-7} kg/kg) for aerosol components and vertical wind fields at NBURG air quality stations.

4. Summary

A multi-data set approach is used to analyze two long-range transport events, one is dust-dominated event in Northern Taiwan, and the other is an annually occurring less extreme smoke events originating from western North America to NYS. The transport of smoke aerosols was analyzed using multiple datasets and model results, including trajectory simulations, the MERRA-2 reanalysis, space-borne and ground-based observations.

For the dust-dominated event in Northern Taiwan, deep trough provided an efficient downwind motion, brought dust from upper levels to the surface and pushed dust southeastward. For the smoke event in NYS, it came with frontal system passing by and had less air quality impact in NYS. However, as the cold front move to the southeast NYS, the convective transport brought precipitations and smoke plumes aloft mixed down to the surface, which enhanced surface $PM_{2.5}$ concentration.

Based on two long-range aerosol transport scenarios, the impact on surface air quality is largely determined by whether there are favorable conditions for mixing aloft dust or smoke aerosols down to the surface. Instead of high-pressure system with stable weather condition, the convective transport from the frontal system also provide downward motion which is favor of aerosol plumes subsidence down to the surface.

References

Bertschi, I. T., and D. A. Jaffe (2005), Long-range transport of ozone, carbon monoxide, and aerosols to the NE Pacific troposphere during the summer of 2003: Observations of smoke plumes from Asian boreal fires, *110*(D5), doi:doi:10.1029/2004JD005135.

Bond, T. C., D. G. Streets, K. F. Yarber, S. M. Nelson, J.-H. Woo, and Z. Klimont (2004), A technology-based global inventory of black and organic carbon emissions from combustion, *109*(D14), doi:doi:10.1029/2003JD003697.

Bory, A. J. M., P. E. Biscaye, and F. E. Grousset (2003), Two distinct seasonal Asian source regions for mineral dust deposited in Greenland (NorthGRIP), *Geophysical Research Letters*, *30*(4), doi:10.1029/2002GL016446.

Buchard, V., et al. (2017), The MERRA-2 Aerosol Reanalysis, 1980 Onward. Part II: Evaluation and Case Studies, *Journal of Climate*, *30*(17), 6851-6872, doi:10.1175/JCLI-D-16-0613.1.

Chen, S.-P., C.-H. Lu, J. McQueen, and P. Lee (2018), Application of satellite observations in conjunction with aerosol reanalysis to characterize long-range transport of African and Asian dust on air quality in the contiguous U.S, *Atmospheric Environment*, *187*, 174-195, doi:https://doi.org/10.1016/j.atmosenv.2018.05.038.

Colarco, P., A. da Silva, M. Chin, and T. Diehl (2010), Online simulations of global aerosol distributions in the NASA GEOS-4 model and comparisons to satellite and ground-based aerosol optical depth, *115*(D14), doi:doi:10.1029/2009JD012820.

Colarco, P. R., M. R. Schoeberl, B. G. Doddridge, L. T. Marufu, O. Torres, and E. J. Welton (2004), Transport of smoke from Canadian forest fires to the surface near Washington, D.C.: Injection height, entrainment, and optical properties, *109*(D6), doi:doi:10.1029/2003JD004248.

Crutzen, P. J., and M. O. Andreae (1990), Biomass Burning in the Tropics: Impact on Atmospheric Chemistry and Biogeochemical Cycles, *250*(4988), 1669-1678, doi:10.1126/science.250.4988.1669 %J Science.

Crutzen, P. J., L. E. Heidt, J. P. Krasnec, W. H. Pollock, and W. Seiler (1979), Biomass burning as a source of atmospheric gases CO, H2, N2O, NO, CH3Cl and COS, *Nature*, *282*(5736), 253-256, doi:10.1038/282253a0.

Damoah, R., N. Spichtinger, C. Forster, P. James, I. Mattis, U. Wandinger, S. Beirle, T. Wagner, and A. Stohl (2004), Around the world in 17 days - hemispheric-scale transport of forest fire smoke from Russia in May 2003, *Atmos. Chem. Phys.*, *4*(5), 1311-1321, doi:10.5194/acp-4-1311-2004.

Darmenov, A., and A. M. da Silva (2015), The Quick Fire Emissions Dataset (QFED) – Documentation of versions 2.1, 2.2 and 2.4*Rep.*, 211 pp.
Draxler, R. R., and G. D. Rolph (2012), Evaluation of the Transfer Coefficient Matrix (TCM) approach to model the atmospheric radionuclide air concentrations from Fukushima, *117*(D5), doi:doi:10.1029/2011JD017205.
EPA, U. (2012), Our Nation's Air—Status and Trends through 2010*Rep.*
Forster, C., et al. (2001), Transport of boreal forest fire emissions from Canada to Europe, *106*(D19), 22887-22906, doi:doi:10.1029/2001JD900115.
Gelaro, R., et al. (2017), The Modern-Era Retrospective Analysis for Research and Applications, Version 2 (MERRA-2), *Journal of Climate*, *30*(14), 5419-5454, doi:10.1175/JCLI-D-16-0758.1.
Hsu, S.-C., et al. (2012), Dust transport from non-East Asian sources to the North Pacific, *39*(12), doi:10.1029/2012gl051962.
Jaffe, D., I. Bertschi, L. Jaeglé, P. Novelli, J. S. Reid, H. Tanimoto, R. Vingarzan, and D. L. Westphal (2004), Long-range transport of Siberian biomass burning emissions and impact on surface ozone in western North America, *31*(16), doi:doi:10.1029/2004GL020093.
Jung, J., J. Yu, Y. Lyu, M. Lee, T. Hwang, and S. Lee (2017), Ground-based characterization of aerosol spectral optical properties of haze and Asian dust episodes under Asian continental outflow during winter 2014, *Atmos. Chem. Phys.*, *17*(8), 5297-5309, doi:10.5194/acp-17-5297-2017.
Laszlo, I., and H. Liu (2016), NOAA NESDIS Center for Satellite Applications and Research: EPS Aerosol Optical Depth (AOD) Algorithm Theoretical Basis Document*Rep.*
Leung, F.-Y. T., J. A. Logan, R. Park, E. Hyer, E. Kasischke, D. Streets, and L. Yurganov (2007), Impacts of enhanced biomass burning in the boreal forests in 1998 on tropospheric chemistry and the sensitivity of model results to the injection height of emissions, *112*(D10), doi:doi:10.1029/2006JD008132.
Levine, J., W. R. Iii Cofer, D. Cahoon, and E. Winstead (1995), *Biomass burning a driver for global change*.
Lin, C.-Y., et al. (2012), Impact of different transport mechanisms of Asian dust and anthropogenic pollutants to Taiwan, *Atmospheric Environment*, *60*, 403-418, doi:https://doi.org/10.1016/j.atmosenv.2012.06.049.
Liu, C.-M., C.-Y. Young, and Y.-C. Lee (2006), Influence of Asian dust storms on air quality in Taiwan, *Science of The Total Environment*, *368*(2), 884-897, doi:https://doi.org/10.1016/j.scitotenv.2006.03.039.
Liu, M., D. L. Westphal, S. Wang, A. Shimizu, N. Sugimoto, J. Zhou, and Y. Chen (2003), A high-resolution numerical study of the Asian dust storms of April 2001, *108*(D23), doi:10.1029/2002jd003178.
Mori, I., M. Nishikawa, T. Tanimura, and H. Quan (2003), Change in size distribution and chemical composition of kosa (Asian dust) aerosol during long-range transport, *Atmospheric Environment*, *37*(30), 4253-4263, doi:https://doi.org/10.1016/S1352-2310(03)00535-1.
Petzold, A., et al. (2007), Perturbation of the European free troposphere aerosol by North American forest fire plumes during the ICARTT-ITOP experiment in summer 2004, *Atmos. Chem. Phys.*, *7*(19), 5105-5127, doi:10.5194/acp-7-5105-2007.
Randles, C. A., et al. (2017), The MERRA-2 Aerosol Reanalysis, 1980 Onward. Part I: System Description and Data Assimilation Evaluation, *Journal of Climate*, *30*(17), 6823-6850, doi:10.1175/JCLI-D-16-0609.1.
Seiler, W., and P. J. Crutzen (1980), Estimates of gross and net fluxes of carbon between the biosphere and the atmosphere from biomass burning, *Climatic Change*, *2*(3), 207-247, doi:10.1007/BF00137988.
Stein, A. F., R. R. Draxler, G. D. Rolph, B. J. B. Stunder, M. D. Cohen, and F. Ngan (2015), NOAA's HYSPLIT Atmospheric Transport and Dispersion Modeling System, *Bulletin of the American Meteorological Society*, *96*(12), 2059-2077, doi:10.1175/BAMS-D-14-00110.1.
Tsai, F., G. T.-J. Chen, T.-H. Liu, W.-D. Lin, and J.-Y. Tu (2008), Characterizing the transport pathways of Asian dust, *113*(D17), doi:10.1029/2007jd009674.
Tsai, F., J.-Y. Tu, S.-C. Hsu, and W.-N. Chen (2014), Case study of the Asian dust and pollutant event in spring 2006: Source, transport, and contribution to Taiwan, *Science of The Total Environment*, *478*, 163-174, doi:https://doi.org/10.1016/j.scitotenv.2014.01.072.
Wang, S.-H., W.-T. Hung, S.-C. Chang, and M.-C. Yen (2016), Transport characteristics of Chinese haze over Northern Taiwan in winter, 2005–2014, *Atmospheric Environment*, *126*, 76-86, doi:https://doi.org/10.1016/j.atmosenv.2015.11.043.
Wang, X., Z. Dong, J. Zhang, and L. Liu (2004), Modern dust storms in China: an overview, *Journal of Arid Environments*, *58*(4), 559-574, doi:https://doi.org/10.1016/j.jaridenv.2003.11.009.
Wu, Y., A. Arapi, J. Huang, B. Gross, and F. Moshary (2018), Intra-continental wildfire smoke transport and impact on local air quality observed by ground-based and satellite remote sensing in New York City, *Atmospheric Environment*, *187*, 266-281, doi:https://doi.org/10.1016/j.atmosenv.2018.06.006.
Zhang, H., S. Kondragunta, I. Laszlo, H. Liu, L. A. Remer, J. Huang, S. Superczynski, and P. Ciren (2016), An enhanced VIIRS aerosol optical thickness (AOT) retrieval algorithm over land using a global surface reflectance ratio database, *Journal of Geophysical Research: Atmospheres*, *121*(18), 10,717-710,738, doi:10.1002/2016JD024859.